Movement and force produced by a single myosin head

J. E. Molloy, J. E. Burns, J. Kendrick-Jones*, R. T. Tregear* & D. C. S. White

Department of Biology, University of York, York YO1 5DW, UK
*Laboratory of Molecular Biology, Hills Road, Cambridge CB2 2QH, UK

MUSCLE contraction is driven by the cyclical interaction of myosin with actin, coupled to the breakdown of ATP. Studies of the interaction of filamentous myosin[1] and of a double-headed proteolytic fragment, heavy meromyosin (HMM)[2,3], with actin have demonstrated discrete mechanical events, arising from stochastic interaction of single myosin molecules with actin. Here we show, using an optical-tweezers transducer[2,4], that a single myosin subfragment-1 (S1), which is a single myosin head, can act as an independent generator of force and movement. Our analysis accounts for the broad distribution of displacement amplitudes observed, and indicates that the underlying movement (working stroke) produced by a single acto-S1 interaction is ~4 nm, considerably shorter than previous estimates[1-3,5] but consistent with structural data[6]. We measure the average force generated by S1 or HMM to be at least 1.7 pN under isometric conditions.

Previous studies[7-9], under conditions in which several molecules are interacting with the actin filament, indicated that both S1 and single-headed myosin are capable of generating movement and force. To demonstrate that such events occur between a single myosin head and an actin monomer, we have measured interactions between S1 and actin using an optical-tweezers apparatus[5]; its means of operation is similar to that used previously[2], except that it synthesizes a double trap by rapid scanning of a single laser beam, and has a position detector with a frequency response high enough (2.2 kHz) to allow observation of the full amplitude of brownian motion.

An actin filament was suspended between two polystyrene beads held in optical traps, and its intermittent interaction with S1 or HMM bound to a stationary glass sphere at low surface density was monitored by measuring the motion of one of the beads (see Fig. 1 legend). The surface concentration of S1 or HMM and the bulk concentration of ATP were chosen so that mechanical interactions between a single S1 head and the actin filament could be readily observed.

When low concentrations of either S1 or HMM were used, fast-rising displacements could be clearly distinguished from thermal vibration of the actin filament (Fig. 1*a–c*). Most of the displacements were in one direction, but negative displacements were also observed (down arrows). By rotating the two trap positions through 180° about the myosin contact, so that the polarity of the actin filament was reversed, we found that the preferred direction of the displacements was also reversed and that ~80% of displacements occurred in the preferred direction. In 10 μM ATP, the average duration of positive and negative displacements was 90 ms and was independent of the amplitude of the observed attachment (Fig. 1*g*), suggesting that the presence of a preferred direction for attachment is not a kinetic effect arising from differences in probability of detachment, but is probably due to a myosin work stroke with its polarity determined by that of the actin filament. Lowering the ATP concentration from 10 μM (Fig. 1*b*) to 2 μM (Fig. 1*c*) increased the mean duration. Those amplitudes of positive and negative displacements which could be distinguished from thermal noise were measured from the mean resting position. Histograms of the distribution of measured events are shown for both HMM and S1 in Fig. 2*a*, *b*. The striking feature of our data is the significant number of very large displacements (up to 30 nm) and negative displacements (down to −25 nm). Large-amplitude positive displacements have previously been observed[2,3], especially at low optical trap stiffness, but negative displacements had not.

Noise of the displacement records is due to the thermal motion of the bead. During both positive and negative displacement events the amplitude of brownian noise was reduced, indicating that system stiffness had increased (Fig. 1*a–c*). Particularly in traces obtained at 5 and 2 μM ATP, periods of low noise were also observed without significant changes in mean displacement (Fig. 1*c*). S1 stiffness, κ_m, predicted from noise analysis during these periods, was similar irrespective of displacement ($\kappa_{xm} - \kappa_x = 0.48$ pN nm^{-1}).

Using low variance of noise (Fig. 1*d*) as the criterion for attachment, we again measured the size of displacements produced by S1 and HMM relative to the mean rest position. In contrast to the method above, this technique enabled us to identify work strokes that drove the bead to near its mean position. The resulting histograms are shown in Fig. 2*c*, *d*.

In feedback (force) mode (Fig. 1 legend) the bead was held in a fixed position, the forces exerted by the molecular interactions being compensated by movement of the laser trap, allowing estimates of the isometric forces produced by single acto-myosin interactions (Fig. 3*a*). The mean force of the events was 1.7 pN and their duration was similar to that of the displacements. We found that HMM produced approximately the same amount of force as S1 (Fig. 2*e*, *f*).

Controlled, large-amplitude length changes were applied by imposing movement to the laser beam holding the bead imaged on the photodetector. The forces were measured from the movement of the laser beam required to produce the correct movement of the bead (Fig. 3*b*). The minimum stiffness of a single acto-myosin interaction was determined from the change in force required to produce a given displacement. Mean stiffness, measured from the gradient of length–tension diagrams, was 0.17 pN nm^{-1} (Fig. 3*c*), much less than the above estimates from noise analysis, but stiffer than the trap stiffness used for our estimates of the working stroke, and similar to estimates of crossbridge stiffness in muscle fibres.

The similarity between the displacements and forces produced by S1 and HMM suggests that the same molecular process is generating the mechanical events found in both preparations. The possibility that the S1 measurements might arise from contaminant HMM is excluded by the absence of HMM in gels of the S1 preparation (Fig. 1 legend) and the fact that only three times more S1 was needed than HMM to produce these mechanical results. We conclude that a single myosin head can generate force and movement.

To extract the size of the working stroke from our data, the randomizing effect of thermal filament displacement has to be considered. We believe that crossbridge attachment will occur with equal intrinsic probability over the full range of the brownian motion of the actin filament. The start position of the myosin molecule relative to the bead rest position is arbitrary, certainly between different bead/actin filament preparations, and probably to some extent between records using any particular actin filament. The actin filament is free to rotate in an unconstrained fashion, so on average every actin monomer must be equivalent. The beads and actin filament would be expected to rotate over several seconds[10] (that is, the period of a single recording). Thus dependence of attachment upon azimuthal orientation[5] will be detectable only in recordings made with sufficient speed. Different recordings will have different azimuthal start points. Although summation of mechanical events will be very rare at the dilutions of protein used, there is likely to be more than one S1 head able to interact with the actin filament over the time scale of these experiments.

Our interpretation of the distribution of displacements in Fig. 2*a*, *b* is that crossbridge attachments occur at any axial position of the actin filament, and that the working stroke produces a displacement from that arbitrary starting point. The distribution

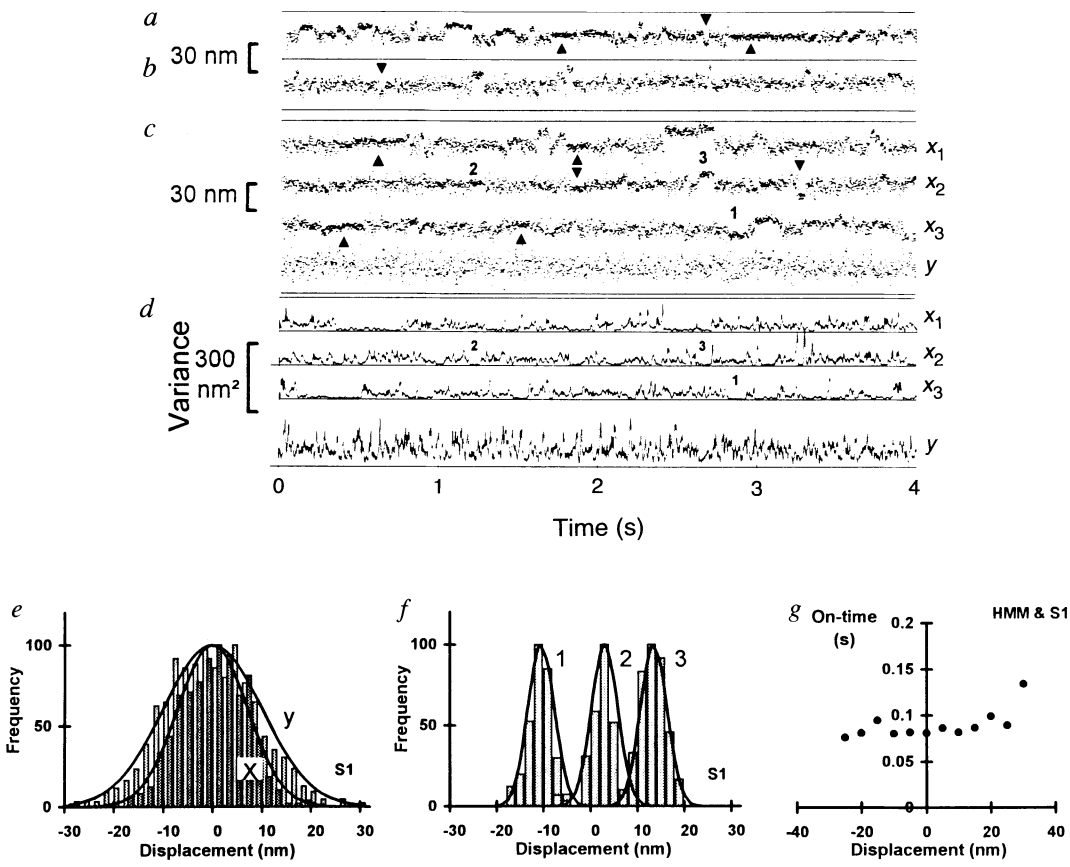

FIG. 1 Displacement of actin filament under near-zero load conditions resulting from interactions with low densities of *a*, HMM and *b–f*, S1. *a*, Record obtained on contact of HMM (bound to surface at 2 μg ml^{-1}) with an actin filament in 10 μM ATP; κ_{trap}, 0.022 pN nm^{-1}. *b*, Similar record obtained with S1, at density of 5 μg ml^{-1}, in 10 μM ATP; κ_{trap}, 0.021 pN nm^{-1}. *c*, Three sequential records (x_1–x_3) obtained on contact of S1 heads, at 6 μg ml^{-1}, with an actin filament in 2 μM ATP; κ_{trap}, 0.042 pN nm^{-1}. The 'noise' content of these records is due to residual brownian motion of the trapped bead. Detector noise was small by comparison (0.8 nm r.m.s.). Note the reduction in thermal vibration during the displacements. Negative displacements marked with down-pointing arrows. Periods showing long low thermal noise and little change of mean position are marked with up-pointing arrows. The fourth trace (*y*) is the record obtained in the *y*-axis during the sampling of x_1. Sampling frequency 10 kHz, 5-point average. *d*, Running 13-point variance of the traces in *c*. The gridlines are the zero-axis for the trace immediately above that line. *e,f*, Histograms of the distribution of displacements during the records shown in *c*. *e*, The distribution in the *y*-axis and in the *x*-axis during a 'high-noise' section of the trace. The lines are Boltzmann distributions with zero mean and stiffness $\kappa_y = 0.04$ pN nm^{-1} and $\kappa_x = 0.08$ pN nm^{-1}. The data indicate that the compliance in the *x*-direction is half that in the *y*-direction ($\kappa_x = 2\,\kappa_y$ (see Methods)). This *y*-axis stiffness is very similar to that determined by other means for a single bead. *f*, The distribution during the 'low-noise' sections marked 1, 2 and 3 in *c*. The fitted curves assume a stiffness κ_{xm} of 0.56 pN nm^{-1}. To estimate the amplitude of brownian motion the detector bandwidth must be greater than the brownian noise bandwidth (~600 Hz; controlled by viscous drag on the bead and trap stiffness[12]). Our detector bandwidth (2.2 kHz) was sufficient to estimate the amplitude of brownian noise but gave poor phase information. We were therefore unable to determine accurately the start position of a bead immediately before a crossbridge interaction. *g*, Plot of attached lifetime (on-time) versus displacement during attachment. On-time is nearly independent of displacement polarity and magnitude.

METHODS. S1 was prepared by digestion of rabbit psoas muscle myosin with papain under conditions of low salt and high magnesium; the reaction was stopped with E64 and the supernatant column-purified. The S1 ran as a single peak on ion-exchange and gel filtration chromatography. All three light chains were present, and there was no sign of HMM in SDS–PAGE. F-actin, HMM and NEM-myosin were prepared by standard methods. To make the 1.1-μm polystyrene beads bind to F-actin irreversibly, they were coated with 1 μg ml^{-1} BSA-TRITC and 10 μg ml^{-1} NEM-treated monomeric myosin. Glass microspheres (1.7 μm diameter) were applied to a coverslip as a suspension in 0.1% nitrocellulose; after drying, the coverslip was made part of a 0.2-mm deep flow chamber and S1 was bound in a low ionic strength solution (in mM: 25 KCl, 10 Tris, pH7, 4 $MgCl_2$, 1 EGTA). Rhodamine–phalloidin labelled F-actin and NEM-myosin labelled polystyrene beads were introduced in an ATP-containing *in vitro* motility assay buffer[13] at 23 °C. Two NEM-coated beads were captured by optical traps and an actin filament strung between them. The position of one bead was monitored by brightfield microscopy, using a four-quadrant photodetector[2]. A glass microsphere (coated with S1 or HMM) was brought up close to the actin filament and the interaction with S1 or HMM observed. Each optical trap imposes a trap-stiffness κ_{trap} to its bead, the value of which can be set by varying the laser power. The actin filament stiffness in tension (as is the case in these experiments) is sufficiently great for the 10-μm lengths used[14] that it can be considered rigid. The axial (*x*-axis) system stiffness κ_x) is thus double the individual trap stiffness ($\kappa_x = 2\,\kappa_{trap}$). When a myosin head attaches, its stiffness, κ_m, adds to provide a total stiffness $\kappa_{xm} = \kappa_x + \kappa_m$. The *y*-axis stiffness κ_y will, under all conditions, be approximately equal to κ_{trap}. The mean square deviation from the rest position in the absence of acto-myosin interaction is related to the system stiffness ($\langle x^2\rangle = kT/\kappa_x$; $\langle y^2\rangle = kT/\kappa_{trap}$)[12]. The noise seen on the traces is close to that predicted from the independently derived value of κ_{trap} (Fig. 1*e,f*) and displays a Boltzmann distribution with half-width at half-height $(\ln 2)\,2kT/\kappa_x)^{1/2} \approx 12$ nm for the trap stiffness we have used (see below; Fig. 2*a–d*). κ_{trap} was calibrated using a bead with no actin filament attached (when $\kappa_x = \kappa_y = \kappa_{trap}$) by three methods. First, with the trapped bead held 5 μm from the coverslip a large amplitude triangle wave motion was applied to the microscope slide and Stokes' force[2] ($6\pi\eta av$, with viscosity η, bead radius *a*, stage velocity *v*) produced a bead movement proportional to trap compliance. Second, the mean square brownian motion was measured ($\langle x^2\rangle$) over several seconds at 2.5 kHz bandwidth and the equipartition principle applied ($\frac{1}{2}\kappa_{trap}\langle x^2\rangle = \frac{1}{2}kT$) (ref. 12). Third, the most convenient check of trap stiffness was by on-line power-spectrum analysis using the 3-dB roll-off in brownian noise spectrum ($\nu_c = \kappa/2\pi\beta$; ($\beta = 6\pi\eta a$)[12]; this was measured 5 μm from the coverslip surface. Using this method, laser power was adjusted until data matched a predetermined lorenzian curve. Four-quadrant detector sensitivity was determined by applying a known displacement to the laser tweezer position in the *x*- and *y*-axes. When feedback was applied between the quadrant detector and the optical trap position, stiffness was raised to 5 pN nm^{-1}, measured by applying large Stokes' force. With an actin filament held taut between two trapped beads, κ_x was usually set to be between 0.03 and 0.05 pN nm^{-1}. This stiffness is sufficiently lower than that of the acto-S1 interaction (at least 0.17 pN nm^{-1}; see Figs 1*e, f* and 3*c*) to allow the magnitude of the elementary movement to be estimated.

FIG. 2 *a*, *b*, Frequency distribution of the amplitude of displacements, A_x, scored by measuring displacements that were evident above background of residual brownian noise (*a*, 39 traces from 18 filaments; *b*, 73 traces from 21 filaments). The fits are Boltzmann distributions with $A_x = A_0.\exp\{-\frac{1}{2}\kappa(x-x_0)^2/kT\}$, in which x_0 is the displacement caused by crossbridge interaction. The arbitrary κ and amplitudes were fitted by assuming that all of the data belong to a single distribution in which values are missing for zero and small displacements (for fitting method see *e* below). The crossbridge work stroke, x_0, of these fits is 3.5 nm for S1 and 5.0 nm for HMM. *c*, *d*, Frequency distribution of the amplitude of displacements measured for a more restricted data set (*c*, 9 traces from 4 filaments; *d*, 5 traces from 2 filaments) in which the system was sufficiently stable to estimate crossbridge attachments by the increase in system stiffness (fall in local variance). Using this method, zero and near-zero displacements were quantified (see Fig. 1*c*, *d*). The solid lines have the same values of κ and x_0 as in *a* and *b*, with A_0 scaled to fit the frequency of observations. The broken lines are the best-fit Boltzmann distributions to the data. For S1 the value of x_0 predicted from these data is 3.3 ± 0.73 (s.e.m.) nm and the value of κ is 0.052 pN nm^{-1}. For HMM, $x_0 = 7.9 \pm 0.91$ nm, with $\kappa =$ 0.031 pN nm^{-1}. Note that there are many observations with small or zero displacement. *e*, The data of *a* and *b* were recalculated as log(frequency) versus $(x-x_0)^2$, where x is the observed displacement and x_0 is a constant, thereby causing both 'tails' of the distributions to be positive, and making normal distributions linear, giving a gradient proportional to κ_x and the *y*-intercept of log(A_0). For this calculation, frequencies of 0 or 1 were omitted, as were those for displacements between −7.5 and +10 nm (so only the tails of the histograms were used). The small graphs on the left-hand side show plots of log(frequency) versus $(x-x_0)^2$ for three values of x_0. The main figure shows the value of the regression coefficient of the best linear fit to this relationship versus x_0. The parameters with the highest regression coefficients gave, for S1, $x_0 =$ 3.5 nm, $\kappa = 0.046$ pN nm^{-1}, $A_0 = 131$; and for HMM, $x_0 =$ 5.0 nm, $\kappa = 0.047$ pN nm^{-1}, $A_0 = 126$. Note that, in all cases, the fitted value of κ is very close to the value of κ_x for these experiments. *f*, *g*, Isometric forces from S1 and HMM; amplitude of each event was estimated by eye.

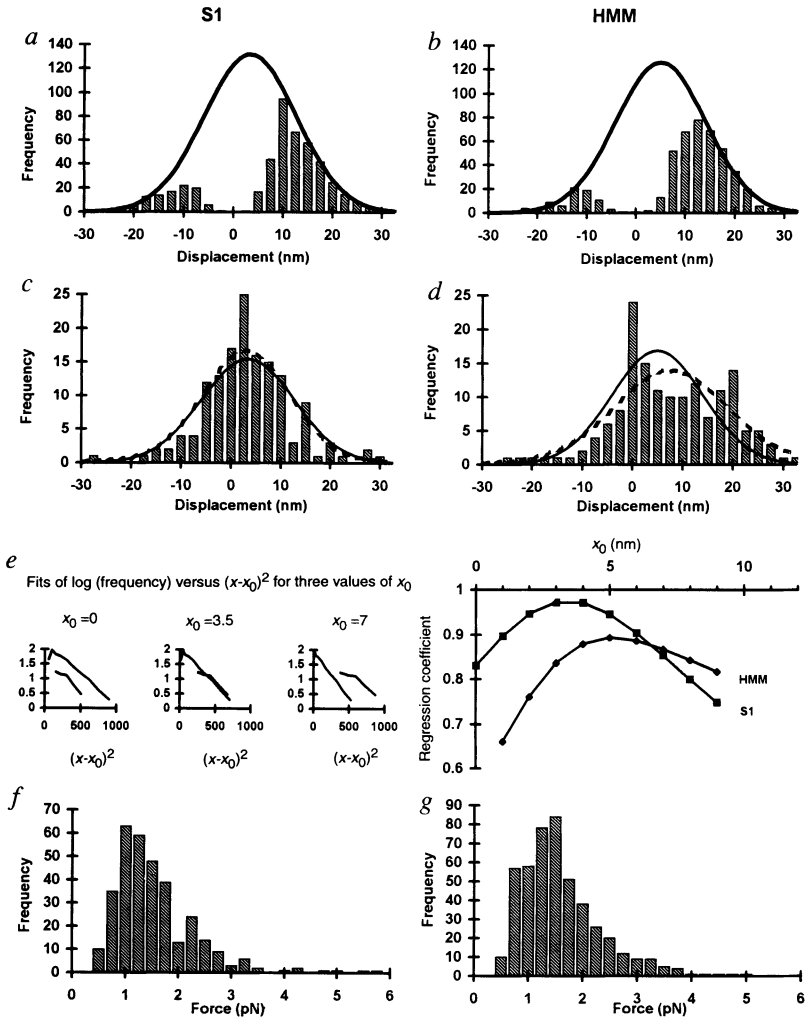

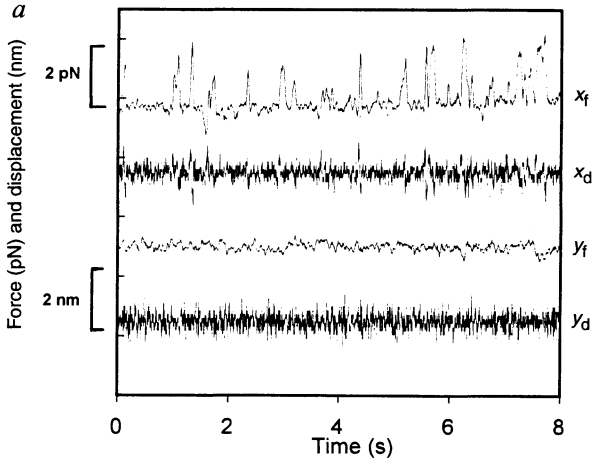

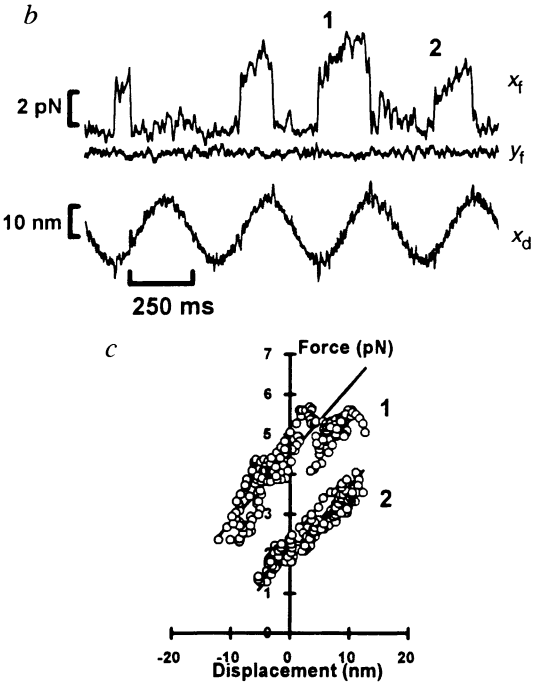

FIG. 3 Force resulting from near-isometric interaction of S1 with actin filaments. 10 μM ATP. *a*, Record of isometric forces. Forces were generated predominantly in one direction, but a few negative forces were detected. Because of the geometry of the optical tweezers, and the fact that only one bead has feedback applied to its position, it is not possible to quantify negative forces. X_f, Y_f; X_d, Y_d: forces and displacements in x and y directions, respectively. *b*, Record of forces with 2.5 Hz, 20 nm forced axial sinusoidal displacement. System stiffness 5 pN nm^{-1}. *c*, Force–extension plot during the marked regions in *b*; fitted lines have a gradient of 0.17 pN nm^{-1} (mean value was 0.17 pN nm^{-1}, $N = 7$ filaments; 25 cyles total).

of displacements will thus have the same half-width as that of the brownian motion in the absence of attachments, but will be shifted by the size of the working stroke (x_0) from the mean rest position. The observed data can be fitted by such a distribution shifted by about 4–5 nm (Fig. 2*a*, *b*). However, observations at or close to zero displacement are missing because, in this and previous analyses[2,3,5], only displacements that deviate clearly from the mean rest position can be scored. The bimodal distribution is simply the two tails of a single broad distribution of crossbridge interactions (Fig. 2*c*, *d*). For S1 the data obtained by scoring attachments (Fig. 2*c*) fit closely to that predicted (solid curve of Fig. 2*a*). For HMM the fit is less good, and it is possible that both heads are contributing to the data observed.

We do not know the extent to which compliance of attachment between S1 and the nitrocellulose substrate acts as an elastic element during force generation; a consequence of this is that our estimates of force and stiffness are lower limits. However, unknown external compliance does not contribute to our estimate of displacement because this is determined from measurements at low force. In addition, the orientation of S1 or HMM on the substrate will presumably be random in these experiments. If the attached head orientates itself with sufficient flexibility that it 'points' in the direction of the actin filament then the above values are correct; however, if the movement produced is determined by its orientation with the substrate then the true value is determined by averaging a cosine term through 180 °, which means that our values of both force and displacement will be underestimates by a factor of $\pi/2$ compared to those measured in muscle-fibre experiments[11]. The finding that the myosin work-stroke size is close to the F-actin monomer repeat is intriguing. Similar findings have been made for kinesin, for which the work stroke seems to be close to the tubulin monomer repeat[12]. □

Received 2 June; accepted 14 September 1995.

1. Ishijima, A. *et al. Biochem. biophys. Res. Commun.* **199,** 1057–1063 (1994).
2. Finer, J. T., Simmons, R. M. & Spudich, J. A. *Nature* **368,** 113–118 (1994).
3. Miyata, H. *et al. J. Biochem., Tokyo* **115,** 644–647 (1994).
4. Ashkin, A., Dziedzic, J. M., Bjorkholm, J. E. & Chu, S. *Optics Lett.* **11,** 288–290 (1986).
5. Molloy, J. E. *et al. Biophys. J.* **68,** 298s–305s (1995).
6. Rayment, I. *et al. Science* **261,** 50–58 (1993).
7. Harada, Y., Noguchi, A., Kishino, A. & Yanagida, T. *Nature* **326,** 805–808 (1987).
8. Toyoshima, Y. Y. *et al. Nature* **328,** 536–539 (1987).
9. Kishino, A. & Yanagida, T. *Nature* **334,** 74–76 (1988).
10. Einstein, A. *Theory of the Brownian Movement* (ed. Furth, R.) (Dover, 1956).
11. Huxley, A. F. & Simmons, R. M. *Nature* **233,** 533–538 (1971).
12. Svoboda, J. K., Schmidt, C. F., Schnapp, B. J. & Block, S. M. *Nature* **365,** 721–727 (1993).
13. Kron, S. J., Toyoshima, Y. Y., Uyeda, T. Q. P. & Spudich, J. A. *Meth. Enzym.* **196,** 399–416 (1991).
14. Kojima, H., Ishijima, A. & Yanagida, T. *Proc. natn. Acad. Sci. U.S.A.* **91,** 12962–12966 (1994).

ACKNOWLEDGEMENTS. We thank J. C. Sparrow, J. D. Currey, S. M. Block and J. Howard for discussions. This work was supported by the Royal Society and BBSRC.

A potential catalytic site revealed by the 1.7-Å crystal structure of the amino-terminal signalling domain of Sonic hedgehog

Traci M. Tanaka Hall*, Jeffery A. Porter†, Philip A. Beachy† & Daniel J. Leahy*‡

* Department of Biophysics and Biophysical Chemistry, and
† Howard Hughes Medical Institute, Department of Molecular Biology and Genetics, Johns Hopkins University School of Medicine, 725 North Wolfe Street, Baltimore, Maryland 21205, USA

WITHIN the past few years, members of the *hedgehog* (*hh*) family of secreted signalling proteins have emerged as the primary signals generated by certain embryonic patterning centres. In vertebrate embryos, for example, *sonic hedgehog* expression in the notochord appears to be responsible for the local and long-range induction of ventral cell types within the neural tube and somites (reviewed in refs 1, 2). Protein products encoded by *hh* family members are synthesized as precursors that undergo autoprocessing to generate an amino-terminal domain that appears to be responsible for both local and long-range signalling activities, and a carboxy-terminal domain that contains the autoprocessing activity[3,4]. As part of an effort to understand how *hh* family members participate in cell-to-cell signalling, we have determined and report here the crystal structure at 1.7 Å of the amino-terminal domain of murine Sonic hedgehog (Shh-N)[5–9]. The structure revealed a tetrahedrally coordinated zinc ion that appears to be structurally analogous to the zinc coordination sites of zinc hydrolases, such as thermolysin and carboxypeptidase A. This previously unsuspected catalytic site represents a distinct activity from the autoprocessing activity that resides in the carboxy-terminal domain.

Crystals of both native and selenomethionyl-substituted (SeMet) Shh-N were grown, and the structure of SeMet Shh-N was determined by the multiwavelength anomalous diffraction (MAD) method[10,11], as summarized in Table 1. The Shh-N structure consists of a core $\alpha+\beta$ sandwich of two α-helices and a six-stranded, mixed β-sheet (β1–β6) decorated by extensive loop regions. A small, two-stranded, antiparallel β-sheet (β′ and β″) is also present. Ribbon drawings and a topology diagram of the Shh-N structure are shown in Fig. 1. This overall fold has not to our knowledge been observed in other proteins. A computer-assisted database search using the program DEJAVU[12] and an extensive search of the SCOP (Structural Classification of Proteins) database[13] failed to identify any similar structures.

After a complete protein model of Shh-N had been built, the original experimentally phased electron-density maps revealed an unexplained peak of more than 11 times the standard deviation of the maps. His 141, Asp 148, His 183 and an apparent water molecule were arranged about this peak in a tetrahedral configuration, and separated from it by distances consistent with metal coordination (Fig. 2*a*). This arrangement is strikingly similar to the coordination of zinc ions in zinc hydrolases such as thermolysin and carboxypeptidase A (Fig. 2*b*), despite otherwise unrelated protein folds[14,15]. In zinc hydrolases, a glutamic acid that is believed to abstract a proton from the zinc-bound water molecule has been shown to be essential for enzymatic activity[16], and an analogous residue, Glu 177, is present in Shh-N. Owing to these similarities, we tested for and confirmed the presence of approximately stoichiometric amounts of zinc in *Escherichia coli*-expressed Shh-N by atomic absorption spectroscopy (data not shown). The structure of Shh-N suggests that the coordinated zinc has a catalytic function, as the zinc in Shh-N is exposed to solvent (Fig. 1*b*) and a water molecule is bound to the zinc in the crystal structure, rather than a fourth amino acid side chain. Structural zinc ions not directly involved in catalysis are generally sequestered from solvent and coordinated by four amino acid side chains that usually include cysteine[16].

In addition to the zinc-coordinating residues and the essential glutamic acid, other residues in thermolysin and carboxypeptidase A are believed to assist in catalysis. An examination of the Shh-N structure reveals residues well positioned to function analogously in Shh-N. These residues include His 135, His 181 and Glu 127 of Shh-N. Figure 2*c* shows a schematic model of the Shh-N zinc site and illustrates how these residues might

‡ To whom correspondence should be addressed.